Construction stresses in the world's first precast concrete network arch bridge

Hossein Yousefpour, Todd A. Helwig, and Oguzhan Bayrak

- The West Seventh Street Bridge in Fort Worth, Tex., built in 2013 and comprising 12 prestressed, precast concrete network arches, was instrumented with vibrating-wire gauges embedded in the arches prior to concrete placement.
- The instrumentation provided data on the stresses induced in the arches during posttensioning, handling, and transport as well as deck construction to ensure no cracking.
- The measurements also provided a means for evaluating the accuracy of stress calculations that were made during design.

Arches provide a structural system that can efficiently support large loads while lending themselves to excellent aesthetics. Historically, arches have been widely used in bridge systems; however, in modern applications, they are usually reserved for signature bridges, where aesthetics play an important role in the design. Because arches primarily resist loads through compression, concrete is an ideal structural material for their application.

While construction techniques and analytical capabilities have systematically improved, relatively few concrete arch bridges were built in the past 50 years,[1] mostly due to their high construction costs. Concrete arches are usually built using timber or steel falsework or cantilever methods, which are time and labor intensive.[2] As a result, structural engineers have been especially interested in improving construction techniques for this efficient, aesthetic structural form.

An innovative solution for constructing concrete arches was used for a signature bridge on West Seventh Street in Fort Worth, Tex. The bridge consists of twelve 280-ton (2500 kN) concrete network arches, which were cast on their sides, rotated into a vertical position, transported, and installed. To withstand the substantial stresses induced by rotation and transportation, the arches were prestressed in both the tie and the rib.

Table 1. Examples of recently constructed steel network arches

Bridge	Country	Arch span length, ft	Year completed
Bugrinsky Bridge	Russia	1247	2014
Troja Bridge	Czech Republic	657	2014
Lake Champlain Bridge	United States	480	2011
The Brandangersundet Bridge	Norway	722	2010
Florabrücke	Germany	435	2010
Blennerhassett Island Bridge	United States	878	2008
Palma del Río Bridge	Spain	427	2008
The Providence River Bridge	United States	400	2007

Note: 1 ft = 0.305 m.

A network arch is a tied arch bridge with inclined hangers, in which each hanger crosses at least two other hangers in the plane of the arch. These densely arranged hangers provide a nearly continuous shear transfer between the rib and the tie and therefore greatly reduce the bending moments and deflections in the arch elements, which results in significant material savings.[3] Network arches were first introduced by Per Tveit in the 1950s as lightweight steel arch bridges with prestressed concrete decks. The world's first network arch bridges, including the Steinkjer Bridge and the Bolstadstraumen Bridge in Norway and the Fehmarn Sound Bridge in Germany, were constructed in the early 1960s. They had span lengths of 262 ft (79.9 m), 275 ft (83.8 m), and 814 ft (248 m), respectively. In the following years, many other steel network arches were built around the world (**Table 1**).[3–15]

Steel network arches are usually constructed using prefabricated segments. Due to their light weight, it is also common to assemble the whole steel skeleton with parts of the deck at a temporary construction site and transport the span into position. A typical construction sequence begins with assembling the tie element and the deck on temporary shoring. In the next step, another temporary structure is constructed on the deck to support the arch rib segments. Once all rib segments are erected and properly connected, the hangers are installed and stressed as needed. To achieve the desired forces in the hangers, a detailed stressing sequence is developed based on finite element simulations.[16] The sequence might require multiple rounds of adjustment. However, due to high static indeterminacy in these structures, the resulting stresses are highly dependent on the modeling assumptions, construction imperfections, and temperature.

The West Seventh Street Bridge, which was completed in 2013, is believed to be the first precast concrete network arch bridge in the world.[17] Despite Tveit's early suggestions to build network arches using high-strength concrete ribs,[3] the authors have not been able to find records of any previously built concrete network arches. Therefore, it is likely that the West Seventh Street Bridge is also the first concrete network arch bridge in the world. Prefabrication of the concrete arches in this project significantly reduced on-site construction time and allowed better quality control. However, the designers predicted that some of the most critical times in the life of the arches happened during construction. As a result, accurately estimating the stresses during construction was critical. While sophisticated finite element models were used to predict the stresses in the structure, the possibility of damaging the arches during construction remained a concern. Therefore, a field monitoring study was initiated to evaluate the performance of the arches during construction. As a part of field monitoring, the arches were instrumented and data were collected and interpreted to ensure the safety of the arches and verify the design assumptions.[18]

This paper presents the findings from the instrumentation of the West Seventh Street Bridge with a focus on short-term stresses during handling. A brief overview of the innovative design of the bridge is presented. The instrumentation, monitoring, and interpretation of data are then described. Finally, comparisons are made between the stresses measured in the structure and those predicted in design calculations.

The West Seventh Street Bridge

The new West Seventh Street Bridge was designed to replace a century-old bridge that connected downtown Fort Worth to the cultural district. The bridge spans four lanes of traffic, the Clear Fork of the Trinity River, and a number of recreational trails.

The aesthetics of the replacement bridge were of importance to city officials. The majority of new bridges in Texas are precast concrete girder bridges, which could also have provided an economical solution for this project. However, the new West Seventh Street Bridge was expected to be a signature bridge and a pleasant gateway to five internationally renowned museums in the cultural district.[17] On the other hand, due to high traffic demands, the new bridge needed to be constructed as quickly as possible.

Site conditions allowed engineers to use six uniform spans of 163.5 ft (49.83 m). Therefore, they conceived an innovative solution comprising 12 identical precast, prestressed concrete network arches. While the decision to use arches was highly influenced by aesthetic considerations, the identical design of all arches and the possibility of precasting resulted in a significant reduction in construction costs and the time of street closure and made precast concrete arches feasible. **Figure 1** shows the layout of a typical span

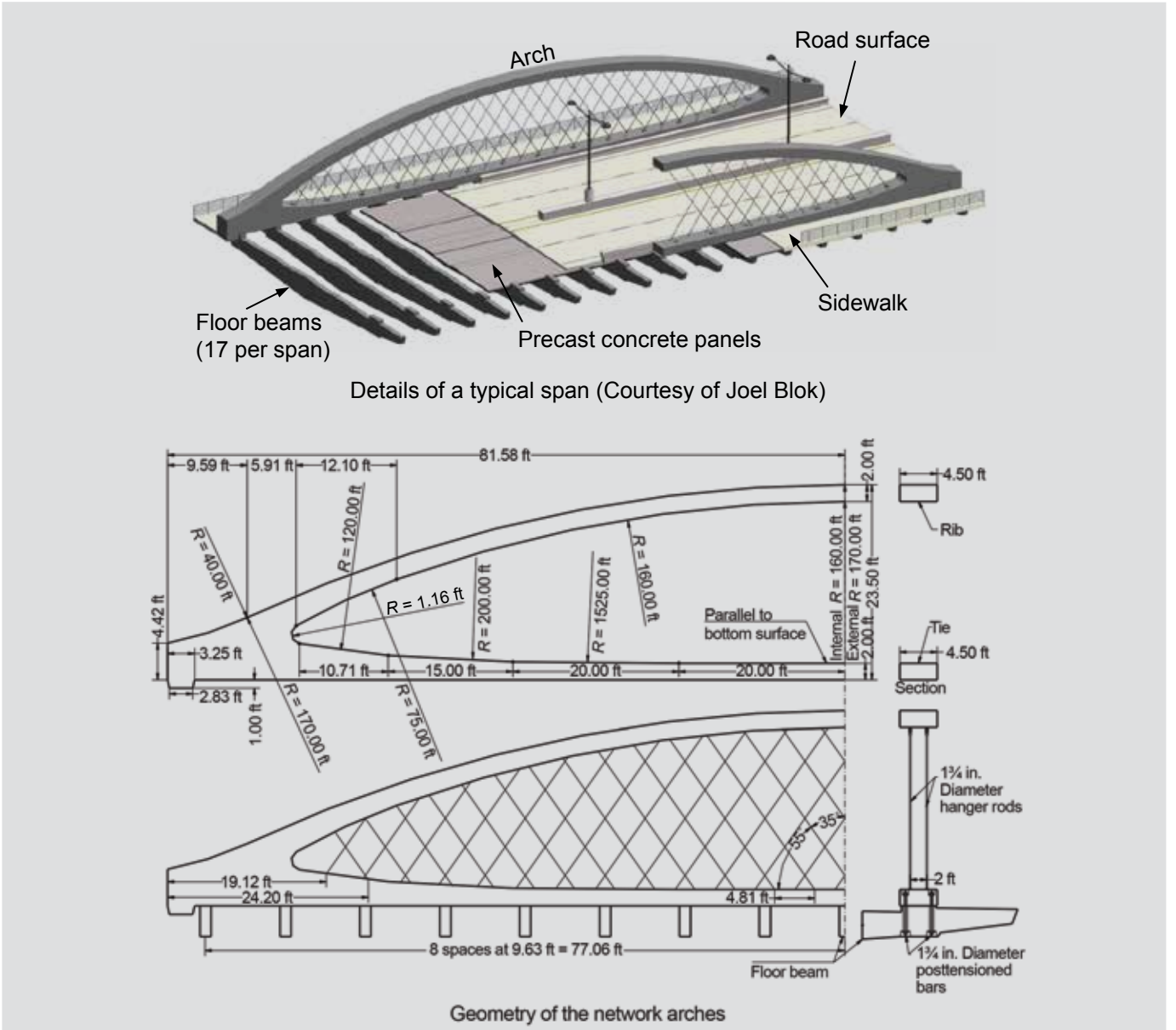

Figure 1. The new West Seventh Street Bridge. Note: R = radius of curvature. 1 in. = 25.4 mm; 1 ft = 0.305 m.

and the detailed geometry of the precast concrete arches. The bridge carries four lanes of traffic and two sidewalks, which are located outside the arches that support the spans. Each concrete arch includes 52 hangers, which are located in two parallel planes, spaced 2 ft (0.6 m) apart (Fig. 1). The 26 hangers in each plane are parallel to each other, all with an angle of 35 degrees from the vertical. However, the hangers in two planes are inclined in opposite directions, resulting in a mesh that is typical of a network arch. The deck is constructed using precast concrete panels with a cast-in-place concrete topping slab and is supported by 17 prestressed concrete floor beams, which are suspended from the arches using posttensioned bars (Fig. 1). The floor beams are pretensioned elements with a nominal depth of 5 ft 6 in. (1.7 m) at midspan, which is tapered to a depth of 3 ft (0.9 m) at the arches and further to 1 ft 9 in. (0.53 m) at the ends. These floor beams are 1 ft 4 in. (0.40 m) wide and are spaced at 9 ft 7½ in. (2.93 m).

The precast concrete arches were fabricated in a casting yard less than 1 mi (1.6 km) from the bridge location. The steps for constructing the arches of the West Seventh Street Bridge were as follows:

1. The arches were cast on their sides. **Table 2** gives the properties of the concrete used in the arches.

2. To prevent cracking during rotation, a first stage of posttensioning was conducted on the arches: two tendons in the rib were stressed to 208 ksi (1430 MPa), and four tendons in the tie were stressed to 104 ksi (717 MPa). Each tendon consisted of nineteen 0.62 in. (16 mm) strands. **Figure 2** shows the posttensioning tendon layout.

3. The hanger elements were installed. Each hanger was passed through a hanger tube in the tie and threaded

Table 2. Properties of the concrete used in the arches

Parameter	Quantity
Required 56-day compressive strength, psi	8000
Target 28-day compressive strength for mixture design, psi	7900
Typical slump, in.	9
Cementitious-material content, lb/ft^3	25.9
Fly ash replacement ratio (Class F), %	25
Water–cementitious material ratio	0.36
Aggregate/cement ratio	4.4
Typical air content, %	1.4

Note: 1 in. = 25.4 mm; 1 ft = 0.305 m; 1 lb = 4.448 N; 1 psi = 6.895 kPa.

into a clevis at the rib. A nut was put at the other end of the hanger and was hand tightened.

4. The arches were rotated into a vertical position using a lifting assembly in which six lifting frames engaged the sides and bottom surface of the rib and the tie. These lifting frames were symmetric about the midspan of the arches (**Fig. 3**). The lifting frames were supported by a gantry system through a series of equalizer beams and lifting ropes above the rib and below the tie. All lifting points were first raised equally. Once clear of the formwork, only the back lifting points (at the rib) were raised, allowing the arch to pivot to its final vertical orientation (**Fig. 4**). After completing the 90-degree rotation, the arch was moved laterally and positioned on temporary supports, each at a distance of 7 ft (2.1 m) from the end of the arch.

5. Because the small gap between the arches in their final position did not allow any posttensioning, all stressing needed to be completed in the precasting yard. Therefore, a second stage of posttensioning was conducted in which the tie tendons were stressed to 208 ksi (1430 MPa) and the rib tendons were detensioned to 104 ksi (717 MPa).

6. To prestress the hangers, an upward jacking operation was conducted (Fig. 4). Hydraulic rams were positioned under the tie at the locations of future floor beams and were simultaneously activated to push the tie up. When the rams were active, the sag was removed from the hangers and the nuts were retightened (Fig. 4). The rams were then deactivated. As a result,

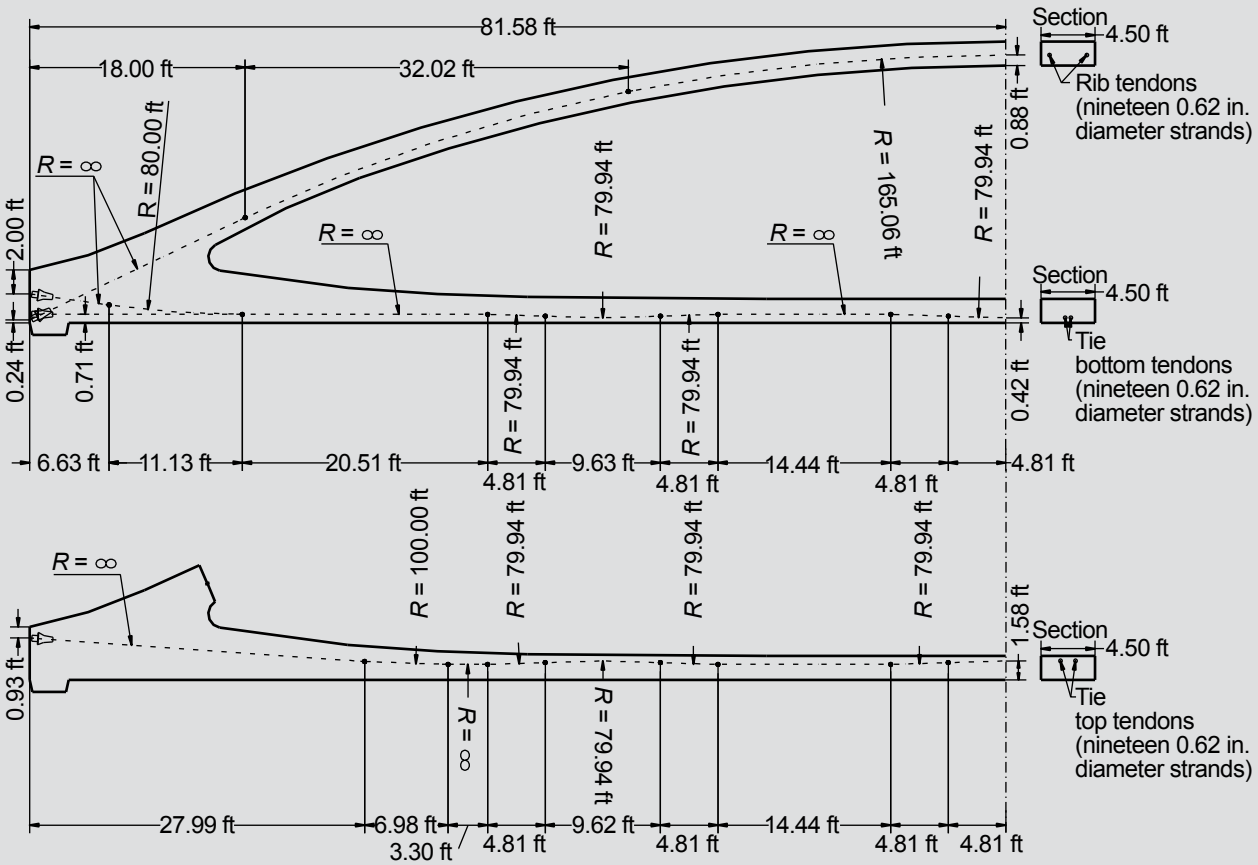

Figure 2. The prestressing layout in the arches. Note: *R* = radius of curvature. 1 in. = 25.4 mm; 1 ft = 0.305 m.

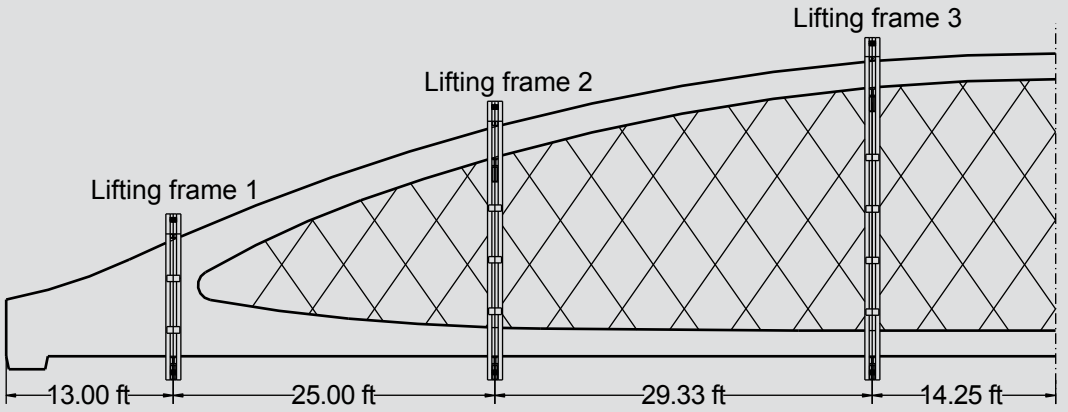

Figure 3. Locations of the lifting frames used for arch rotation. Note: 1 ft = 0.305 m.

the self-weight of the tie induced a prestress in the hangers. To stiffen the rib near the knuckle and prevent excessive tensile stresses during the upward jacking operation, prestressed concrete strongbacks (Fig. 4) were clamped to the rib before upward jacking. These strongbacks remained attached to the arches until all floor beams were installed in each span.

7. Once all arches and new piers were constructed, the arches were moved from the precasting yard to the new piers. Two self-propelled modular transporters carried each arch from the precasting yard to its final location (Fig. 4), where the arch was lifted by cranes and installed on bearings.

8. When all arches were transported to their final locations and properly braced, the street was closed and the old bridge was demolished. The floor beams were then installed, and the construction of the deck for the new bridge began immediately to minimize traffic interruption.

This accelerated construction procedure served to limit the street closure to 120 days. However, because the arches experienced several posttensioning and handling operations, the design team needed to make careful decisions to ensure satisfactory performance of the arches during construction and in service.

To facilitate rotation and transportation, the design team tried to minimize the weight of the arches by making the rib and the tie elements as slender as possible. Moreover, to lower the center of gravity of the arches, a relatively large span-to-rise ratio of 7.6 was used, resulting in a height of only 23.5 ft (7.16 m) at the crown of the arches. Due to the low rise of the arches and also economic and aesthetic considerations, the design included no cross bracing for the rib, but the lateral stability of the bridge is provided by the frame action that is created by moment connections between the two arches and the floor beams.

For design calculations, engineers used an analysis model of the bridge in which the rib and tie elements were modeled using three-dimensional (3-D) thick beam elements. Thick shell elements were used for modeling the knuckle region of the arches. The models also included the effects of staged construction and time-dependent behavior of concrete according to CEB-FIP 1990.[19] The hangers were modeled using 3-D bars. Because the hangers were not expected to resist compressive forces, analysis results were unrealistic when compression was predicted in the hangers. In such cases, the hanger configuration was revised to make sure all hangers remained in tension, and the analysis was repeated.[17]

Using an initial eigenvalue buckling analysis of the uncracked completed structure in the bridge analysis software, the design team predicted the load factor for the lowest buckling mode to be 13.3 for *AASHTO LRFD Bridge Design Speciafications*[20] service I load combination with six lanes of traffic and wind load. The associated buckling mode was the out-of-plane deformation of the rib, with a maximum deformation at the crown. Further studies using nonlinear buckling analyses also showed that with a load factor of 2 for AASHTO LRFD specifications strength III load combination, which is related to transverse wind. The maximum out-of-plane displacement of the rib at the crown was limited to 2 in. (50 mm), and the load-displacement relationship was nearly linear.[17] As a result, the uncracked arches were found to be sufficiently stable against buckling. However, concerns were raised regarding the possibility of cracking during construction.

Cracking is a serviceability concern in most reinforced and prestressed concrete structures. However, potential cracking of the arches during the construction of the bridge could also significantly reduce the stiffness of the rib elements and result in potential out-of-plane instability in the finished bridge, especially because no top lateral bracing was used. Therefore, several measures were taken during design to make sure the arches did not experience excessive tensile stresses so that they would behave like uncracked elements.

Arch rotation

Arrangement of hydraulic rams and strongbacks during upward jacking

Retightening the hanger nuts when the rams were activated

Arch transportation

Figure 4. Construction operations on the precast concrete arches.

The rib is inherently a compressive element. However, the arches were cast horizontally and their ribs were not subjected to compression until the arches were rotated into the vertical orientation. Therefore, excessive tensile stresses in the rib were likely during rotation. The design team chose to minimize the risk of cracking in the rib by stressing the two rib tendons to 208 ksi (1430 MPa) prior to rotation. After rotation, the self-weight of the arches provided some compression in the rib, and the initial prestressing was no longer necessary. However, the stresses due to the self-weight were not large enough to ensure that the ribs remained fully in compression during the remaining construction operations, especially upward jacking. As a result, the designers detensioned the tendons to 104 ksi (717 MPa) after rotation to ensure compression in the arch rib while also avoiding unnecessary prestress. The in-plane stability of the tie element during construction was another important concern. The tie element transfers the horizontal thrust between the supports through tension, and a relatively high prestress is needed to prevent cracking in the tie when the bridge is subjected to service loads. However, the self-weight of the arches generated a small portion of the service load tension in the tie, and as a result, the tie element was subjected to a significant compressive force during the second stage of posttensioning. To avoid potential instability in the tie, the design included a series of small curves in the duct paths so that the tendons would be in contact with the wall of the ducts after a small lateral displacement.[17] As a result, the second-order displacement of the tie was minimized.

While significant efforts were made by the design team to minimize the risk of cracking and prevent instability in the arches, uncertainties existed about the modelling assumptions and the resulting stress calculations, especially because the structure was the first of its kind. On the other hand, the work plan for the arch-handling operations was primarily developed by the contractor and was out of the direct control of the design team. As a result, ensuring that the arches were not experiencing excessive tensile stresses was possible through the instrumentation program highlighted herein.

A vibrating-wire gauge tied to the arch reinforcement

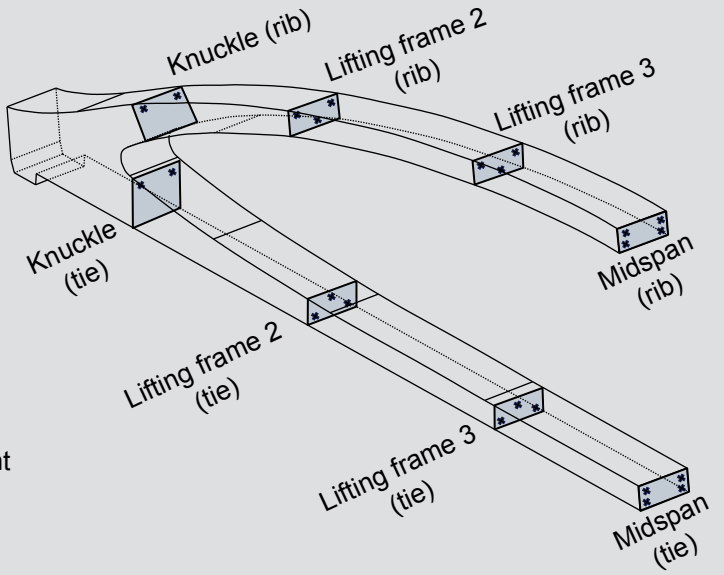

Arrangement of vibrating-wire gauges in different sections of the first two arches

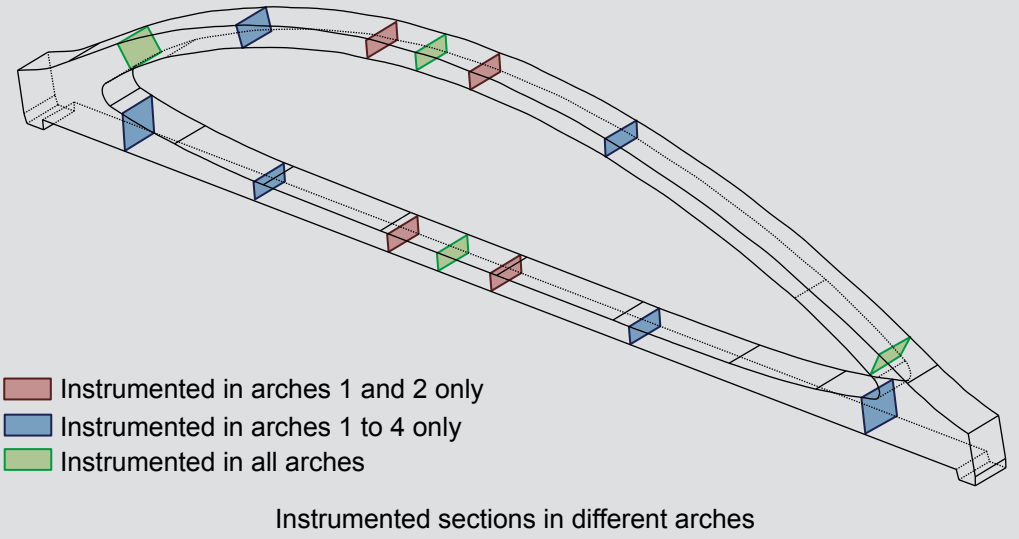

Instrumented sections in different arches

Figure 5. Arch instrumentation details.

Instrumentation

The West Seventh Street Bridge was instrumented using 224 vibrating-wire gauges (VWGs). A VWG includes a strain transducer and a thermistor, which allow for both strain and temperature measurements with resolutions of 1 με and 0.5°C (0.9°F), respectively. The VWGs were installed immediately prior to the assembly of the outside forms for each arch. Each VWG was attached to a no. 3 (10M) steel reinforcing bar, which was tied to the transverse reinforcement of the arch. **Figure 5** shows a VWG installed in the reinforcing cage of one of the arches prior to concrete placement.

Figure 5 also shows the location of the individual VWGs embedded in the first two arches. The instrumented sections were selected in coordination with the design team and included the midspan sections, sections located over the lifting frames during rotation, and sections in the knuckle region. The distribution of the VWGs within each of these sections was selected based on the expected strain profile in the cross section. According to St. Venant's principle, disturbed regions with nonlinear strain distribution are assumed to exist within one member depth from the location of any discontinuity in load or geometry. In other parts of the structure, which are assumed to be nondisturbed, plane sections remain plane and the distribution of strains is linear. In nondisturbed regions, linear interpola-

tion or extrapolation can be used to calculate the strains and stresses at any point in the cross section. However, in disturbed regions, the interpolation or extrapolation of strains is invalid due to the nonlinearity of the strain distribution.[22] The nondisturbed regions of the structure, which included all instrumented sections except those in the knuckle region, were instrumented using three or four VWGs (Fig. 5). As a result, the stresses at every corner of these sections could be found using the plane section assumption. However, for the knuckle region, the strain profile was expected to be highly nonlinear and the VWGs were expected to represent the local strains. Therefore, in these sections, only two VWGs were installed in the anticipated locations of maximum stresses.

The first two arches were instrumented at every section where the designers predicted high stresses so that the safety of the arches could be ensured during construction. The number of instrumented sections was gradually reduced for subsequent arches. Figure 5 shows the instrumented sections in different arches of the bridge.

To improve the flexibility of monitoring for the highly mobile arches, a wireless data-acquisition network was used. The wires from the embedded VWGs were connected to a data-collection box, which received the data and then sent them to the data-acquisition system through wireless communication. The wireless connectivity not only eliminated the lengthy wires on the construction site but also reduced the number of channels needed on the data loggers. The data-acquisition system was also connected to a cellular modem, which enabled remote monitoring of the structure.

The arches were monitored during construction until the bridge was opened to traffic. Depending on the speed of construction activities, different scan rates were used for monitoring the VWGs. The maximum possible scan rate for a single VWG with the available interface analyzers was once every 2 seconds; however, the sensors were scanned sequentially, so the scan rate was reduced. To achieve a suitable scan rate, more data loggers were added to the network when several arches were under construction simultaneously. The resulting configuration allowed the researchers to scan the gauges every 150 seconds, which made it possible to detect changes during rapid construction operations, such as posttensioning. Scanning continued hourly when no construction activity was in progress to capture the effects of temperature fluctuations and time-dependent effects on the structural behavior.

Estimating the mechanical properties of concrete

Realistic values of modulus of elasticity and compressive strength of concrete were essential in processing the data. Therefore, a material test program was conducted to measure the modulus of elasticity E_c and compressive strength f_c' of the concrete used in the arches. To confirm satisfactory placement of concrete in the arches, the contractor constructed a mock-up segment before casting the first arch. The concrete from the mock-up was used to prepare forty-eight 4 × 8 in. (100 × 200 mm) concrete cylinders. All 48 concrete cylinders were tested for modulus of elasticity according to ASTM C469.[23] Because the specimens were loaded only up to 40% of their compressive strength in the modulus test, they were assumed to remain in the elastic range. Therefore, 40 of these cylinders were also tested for compressive strength according to ASTM C39.[24]

The results of these tests were used to develop Eq. (1), which is a mixture-specific equation with a format frequently used to correlate E_c and f_c' for high-strength concrete.[25]

$$E_c = 39\sqrt{f_c'} + 1350 \quad (1)$$

where

E_c = modulus of elasticity of concrete, ksi

f_c' = compressive strength of concrete, psi

To consider the effects of different curing temperatures in the structure compared with test cylinders, the in-situ E_c values were estimated based on the compressive strengths obtained from the maturity method[26] and Eq. (1). The authors used the results of a maturity study by the contractor, which correlated the compressive strength with the maturity of the concrete used in the arches. Using the temperature measurements from VWGs, three average temperatures were calculated at any point in time: the average rib temperature, the average tie temperature, and the average knuckle temperature. Using these temperatures and the results of the maturity study by the contractor, the compressive strength of the concrete was independently calculated for the rib, the tie, and the knuckle. However, because the first construction operation was conducted when the arches were six days old, the difference between the strengths estimated for the rib, the tie, and the knuckle was found to be insignificant during the first stage of posttensioning and later construction operations. Therefore, the average of these three compressive strength values was used to develop a continuous correlation equation for f_c' versus time (Eq. [2]). In developing this mixture-specific equation, a format was implemented that is similar to what was used in a model by Gardner and Lockman, known as GL2000.[27]

$$f_c'(t) = 7500\left(\frac{t^{0.75}}{1.75 + 0.8t^{0.75}}\right) \quad (2)$$

where

t = concrete age after casting, days

This equation was combined with Eq. (1) to estimate the in-situ E_c values at each age. More details related to the procedure for maturity calculations and the development of Eq. (1) and (2) can be found elsewhere.[18]

Processing of data

A considerable processing effort was needed to interpret the data obtained from the instrumentation. The raw data included strains in the VWGs and temperatures at the locations of these sensors, which were used to calculate the stresses at the corners of the instrumented cross sections in the structure.

The first step in stress calculations was to calculate the strains at the corners of the instrumented cross sections. For sections in nondisturbed regions of the arches, plane sections were assumed to remain plane, and strains at any point in the cross section could be calculated using analytic geometry. However, in the disturbed regions of the arches, such as the knuckle region, the distribution of strains was highly nonlinear and therefore the strains could be calculated only at the locations of the VWGs.

The measured strains included several time-dependent and environmental effects, including temperature changes, creep, and shrinkage. These components needed to be excluded from the strain history so that stress-related strains could be multiplied by the modulus of elasticity of the concrete to calculate the stresses.

To minimize the effects of creep and shrinkage in the calculated stresses, the strain changes due to each construction stage were calculated separately and multiplied by the corresponding modulus of elasticity at the time of that construction operation. The total stresses were estimated by adding the stress increments due to each construction operation, as expressed in Eq. (3).

$$\sigma(t) = \sum_{i=1}^{n} E_{ci} \Delta\varepsilon_i \qquad (3)$$

where

E_{ci} = modulus of elasticity of concrete at the time of the i^{th} construction operation

$\Delta\varepsilon_i$ = strain change in concrete due to the i^{th} construction operation

σ = stress in concrete

This method neglects the stress changes that occur when no construction activity is in progress. For example, the effects of prestress losses remain undetected by this method. To include the effects of long-term changes on stresses in the arches, the authors used a more sophisticated data-processing method that incorporates the time-dependent deformations of concrete in stress calculations. However, the effects mentioned will be covered in a later publication and are expected to have a minimal effect on the short-term stress changes that are the focus of the present paper.

In order to eliminate the effects of thermal changes on calculated stresses, the structure was always compared between data points with equal temperatures. During stepwise construction operations, such as posttensioning, the stress changes due to stressing of individual tendons could be calculated because thermal changes during stressing of each tendon were negligible. However, for slower operations, such as arch rotation or transportation, stress changes were obtained by comparing the readings taken during the nights before and after the specific event. Temperature effects were minimized by identifying times before and after the event with equal temperatures. Finding two data points that included exactly the same temperatures at the locations of all VWGs was not practical. However, if the following criteria were satisfied, thermal effects were assumed negligible between the two records: both points were recorded overnight (after sunset and before sunrise) so that the effects of sunlight on nonuniform heating of the arches were minimized; the average temperature of the arch, found from averaging all temperature measurements from the VWG thermistors, was not more than 1°F (0.6°C) different between the two records; and the temperatures from none of the VWG thermistors differed more than 5°F (2.8°C) between the two records.

Results and discussion

Posttensioning response

Figure 6 shows the stress changes in a typical arch during the first stage of posttensioning, and **Fig. 7** shows the stress changes during the second stage of posttensioning on the tie, which was conducted before detensioning the rib tendons. The instrumentation was capable of detecting the stressing of individual tendons inside the rib and the tie. As a result, the recorded data provided the opportunity to evaluate the response of the structure and to check the analytical models of the bridge with respect to each tendon separately. Moreover, the interaction of rib and tie elements could be evaluated by comparing the stress changes in the rib while the tie was being posttensioned and vice versa.

Figures 6 and 7 show that the responses of the arch rib and the tie were relatively independent of each other during posttensioning. For each of the tendons, posttensioning was applied in increments of 52 ksi (360 MPa). During the first

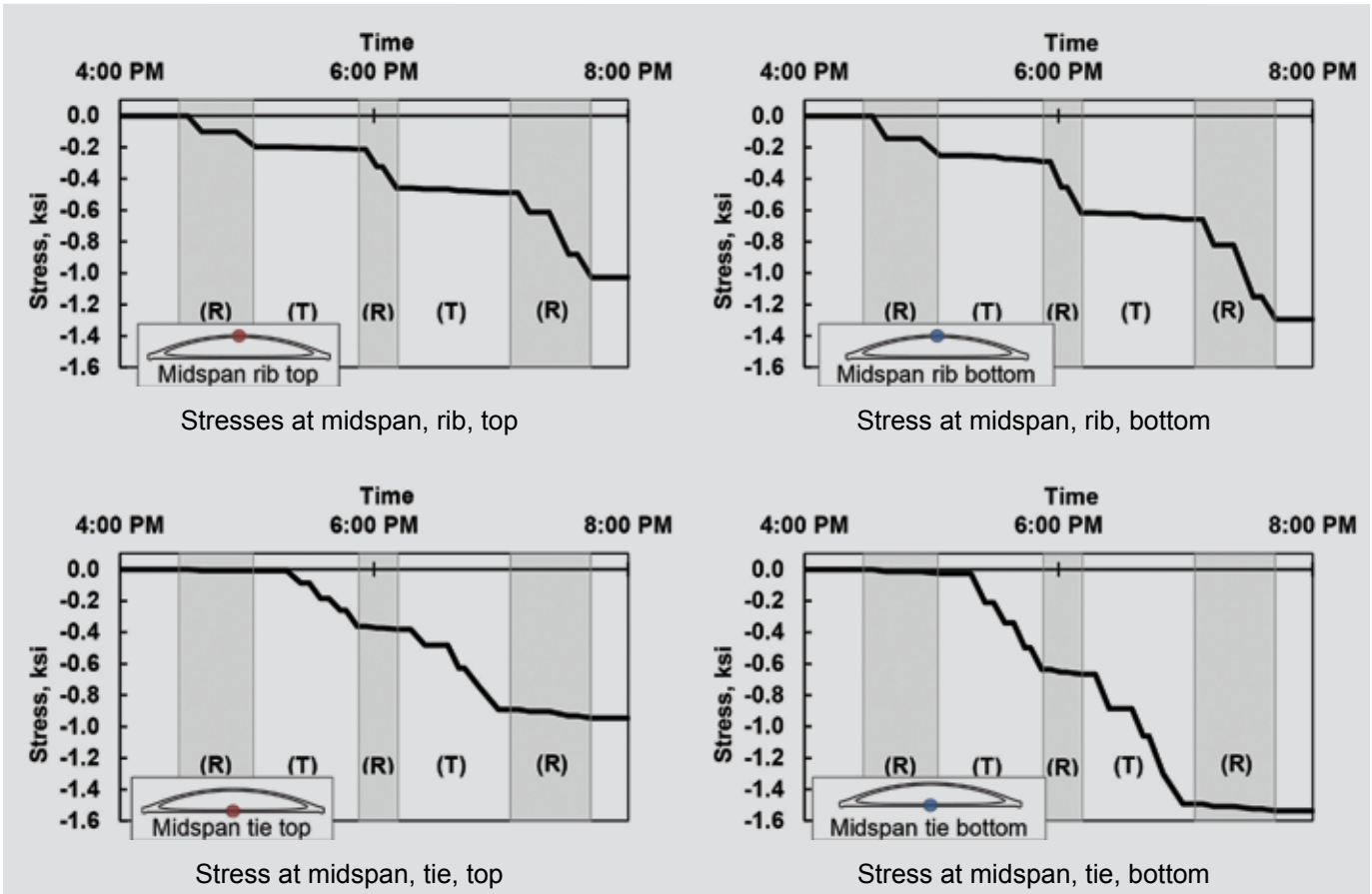

Figure 6. Measured stresses in arch 2 during the first stage of posttensioning. Note: R = prestressing the rib; T = prestressing the tie. 1 ksi = 6.895 MPa.

stage of posttensioning, each increment in the rib tendons increased the stresses at the edges of the rib at midspan by more than 0.10 ksi (0.7 MPa) (Fig. 6 top left, R intervals), but such an increment in the rib caused minimal stress changes at midspan in the tie (Fig. 6 bottom left, R intervals). The maximum stress change anywhere in the tie when a prestress increment was applied to the rib was smaller than 0.02 ksi (0.14 MPa). During the second stage of posttensioning on the tie, stress changes show a similar trend, and negligible stress changes could be observed in the rib (Fig. 7).

The small interaction between the rib and the tie during posttensioning is in contrast with the response of the arches to future external loads. For vertically oriented arches, external dead or live loads mobilize arch action, which induces compression in the rib and tension in the tie to provide static equilibrium with vertical reaction forces at the supports. Posttensioning induces compressive stresses in the rib as well. However, the geometric design of the arches and tendon profiles were carefully chosen so that the anchors for the rib tendons had a relatively small eccentricity from the centroid of the rib. As a result, static equilibrium between internal stresses in the rib and the rib anchorage forces does not require large shear or axial forces in the tie element or significant bending moments in either the rib or the tie. On the other hand, because the bending stiffness of the tie and the rib is much smaller than their axial stiffness, axial deformations happen in each of these elements without inducing noticeable bending stresses in the other. Although the stiff knuckle region provides some local restraint for the deformations of the rib and the tie, the effects of the slight interaction between these elements are mostly limited to the knuckle region and do not materially affect the overall response of the rib or the tie. The authors also observed this behavior through finite element simulations of the arches, which are not within the scope of this paper.

Another important observation was that despite the curved shape of the arch rib, posttensioning did not induce significant bending in this element. This behavior is attributed to the circular profile of the arch and careful selection of the tendon paths and anchorage orientation by the designers. The response of the arch rib to posttensioning is similar to a compressive ring, which is in compression due to the effect of pressure applied along its radius (**Fig. 8**). This characteristic of the arch design was important in reducing the long-term bending deformations in the arch rib under sustained posttensioning forces.

Rotation response

Figure 9 shows the three stages of rotation. The first stage, vertical lifting, occurred when all lifting points were raised

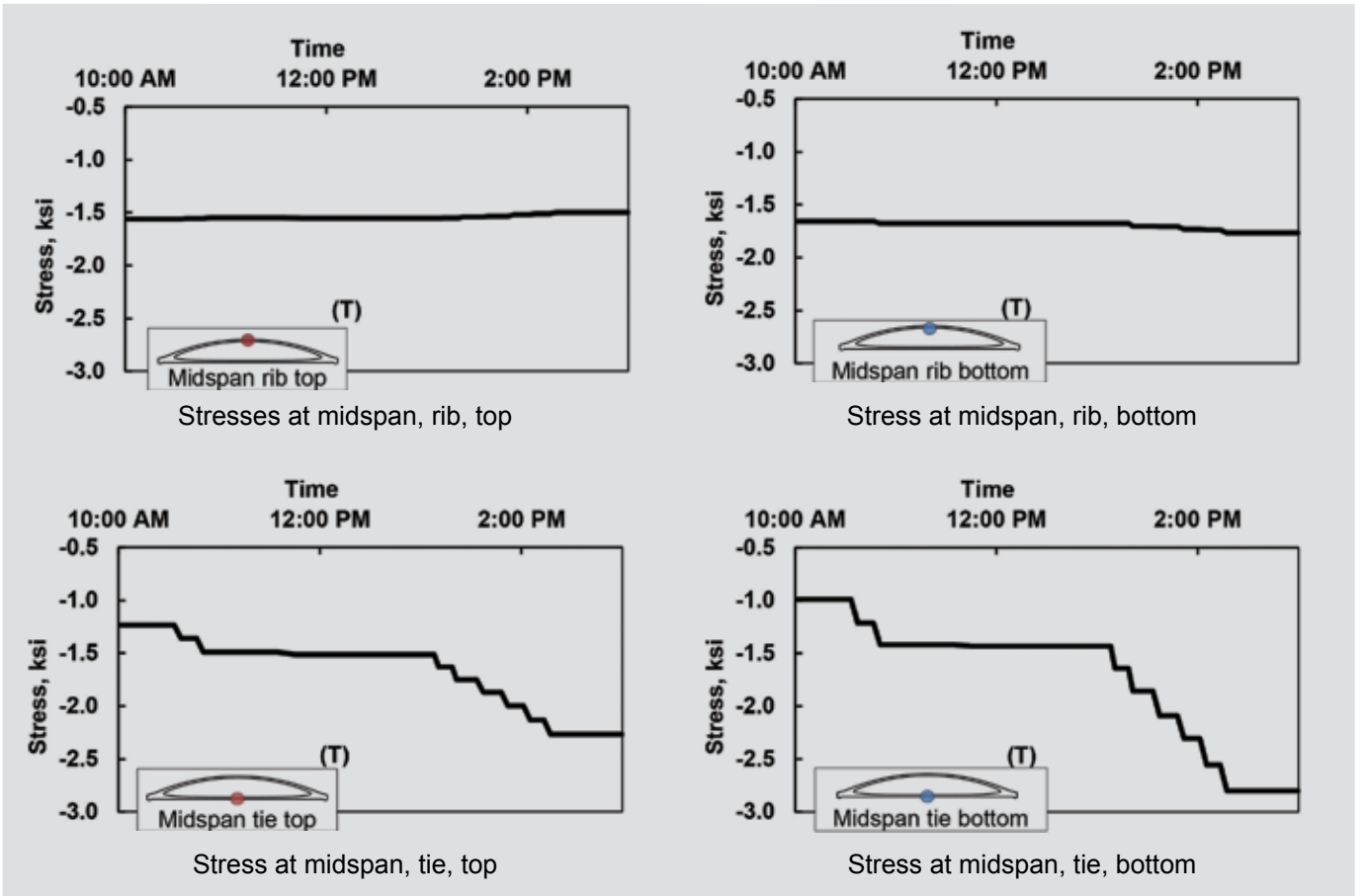

Figure 7. Stresses in arch 2 during the second stage of posttensioning on the tie. Note: T = prestressing the tie. 1 ksi = 6.895 MPa.

equally at the beginning of rotation. The second stage, supported rotation, represents the change of the arch from a horizontal position to a vertical position while the arch was supported by the lifting frames. The third stage, arch setting, represents the release of the arch from the lifting assembly and its installation on temporary supports.

Figure 10 shows typical stress changes at the midspan of arch 2 during the rotation operation. During vertical lifting, the response of the rib and the tie was governed by bending between the lifting frames. However, the magnitude of stress changes during vertical lifting was generally small. Corners A and E (Fig. 10), which were located at the top of the rib and the tie before rotation, experienced an increase in compressive stresses during vertical lifting. Similarly, a decrease in compressive stresses is expected for corners C and G, which were located at the bottom of the rib and the tie before rotation. However, Fig. 10 shows that during vertical lifting of arch 2, corner G experienced an increase in compressive stresses, and the decrease in compressive stresses at corner C is also short lived. In other words, vertical lifting results in an increase in total internal compressive force at the midspan, both in the rib and in the tie. This observation might be due to the interaction between the steel formwork and the arch. During vertical lifting, the arch is released from the bottom formwork, and therefore the friction between the arch and the formwork is eliminated. As a result, local redistribution of the prestressing force could occur in the arches.

The stress changes during supported rotation were gradual and relatively small. Although the arch was loaded by

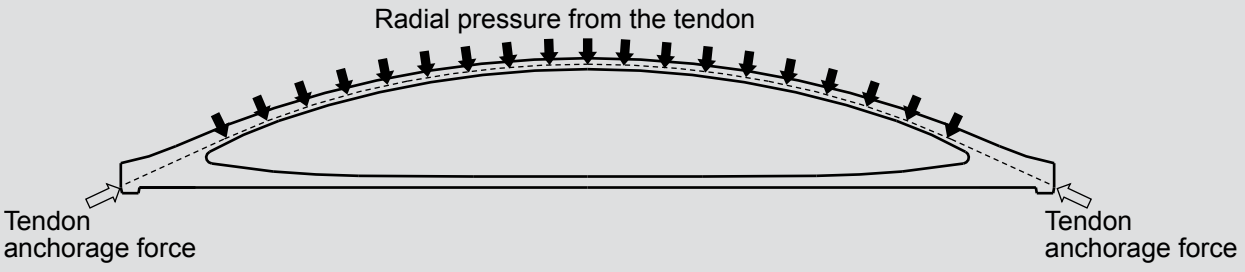

Figure 8. Forces acting on the arch rib due to posttensioning.

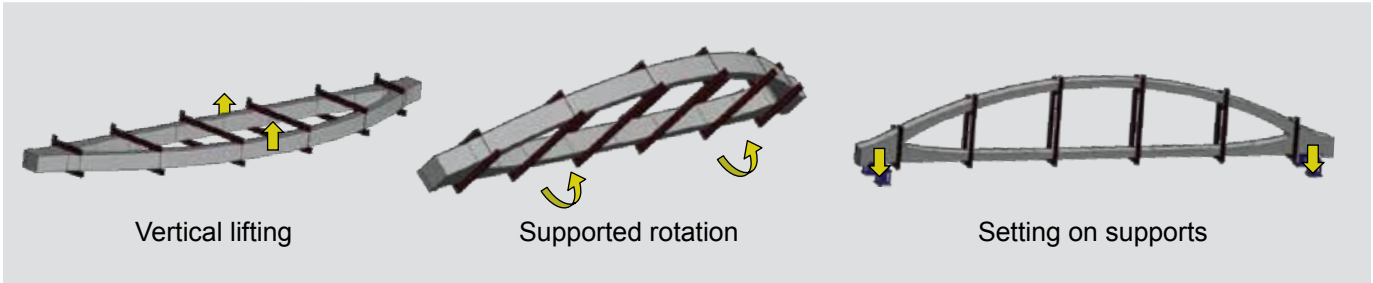

Figure 9. The three stages of the rotation operation.

its self-weight during this stage, it was supported by six lifting frames, which were distributed along the length of the arch, and therefore, the arch action was not mobilized during supported rotation. Most of the observed changes in this stage were caused by the biaxial bending of rib and tie elements as they behaved similarly to continuous beams during supported rotation.

The stress changes during setting of the arch on temporary supports were quick and relatively large. During this stage, the arch action was fully mobilized. Therefore, this stage was associated with a significant increase in compressive stresses in the rib and a significant decrease in those in the tie. Although these stress changes were relatively large, the arches were designed to withstand much larger demands due to bridge deck and live loads in the completed structure. As a result, the arches easily tolerated these stresses in the vertical orientation. Consequently, monitoring the stresses during supported rotation was more critical for ensuring the safety of the arches.

To calculate the stresses during rotation, the construction engineering team developed models of the arches in which the rib and the tie were modeled using tapered beam elements while shell elements were used to model the knuckle region. To obtain more realistic results, the models also included all lifting frames, wire ropes, and equalizer beams that were used for lifting and rotating the arches. To consider the dynamic effects, an amplification factor of 1.5 was also applied to all dead loads.

Figure 11 shows maximum and minimum stresses observed in the arches during supported rotation. None of the arches experienced tension under this operation, and therefore the arches remained crack-free during rotation. The measured stresses were in reasonable agreement with

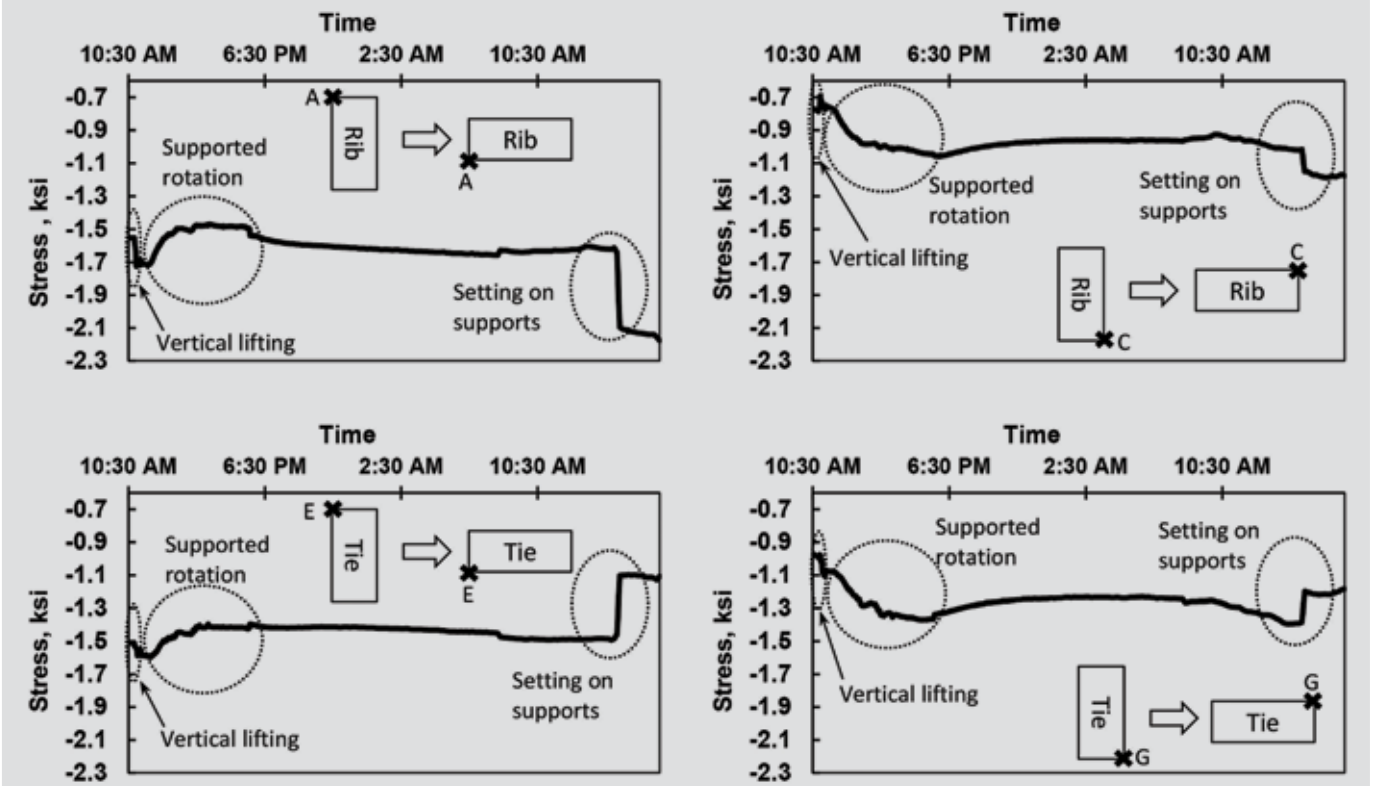

Figure 10. Stress changes at midspan in the rib and the tie during rotation. Note: In each graph, the × shows the corner for which the stress is plotted. 1 ksi = 6.895 MPa.

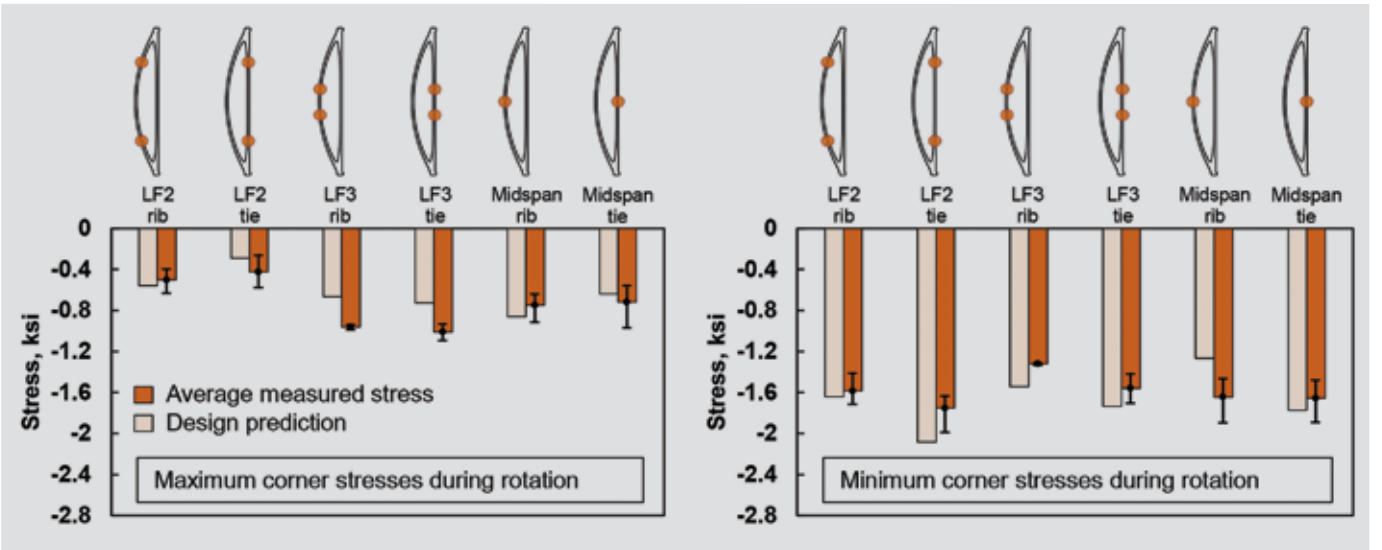

Figure 11. Maximum and minimum corner stresses during the supported rotation of the arches. Note: The black lines show the range of observed stresses in different arches. 1 ksi = 6.895 MPa.

the calculations by the construction engineering team, and where a difference exists between measured and predicted stresses, the predicted response generally overestimated the risk of cracking.

The rotation operation was conducted slowly, and VWG strain records and site observations gave no indication of considerable dynamic effects during rotation. There is a possibility that the 50% increase in the self-weight of the arch in the calculations has contributed to obtaining more realistic stresses. However, additional detailed analysis is needed to draw conclusions that could potentially be used for other projects.

Upward jacking

The upward jacking operation was the most critical stage for the knuckle region of the arches. The design team had predicted that when the hydraulic rams were activated during upward jacking, tension would have been induced at the top of the rib in the knuckle region if the arches had not been temporarily strengthened. Therefore, monitoring the stresses during upward jacking was of critical importance in ensuring their safety against cracking.

Figure 12 shows measured stresses in the arches when the hydraulic rams were activated, but the hanger nuts were not retightened. The stresses in the knuckle region were in agreement with the design predictions. However, as illustrated by the black lines, the variability of stresses among different arches was relatively large. While the average measured stress at the top of the rib in the knuckle was compressive, some arches experienced tension in this region. These tensile stresses were well below the modulus of rupture of the concrete and therefore did not pose any risk of cracking to the arches. The stresses at the midspan of the arches in the tie were also highly variable (Fig. 12). The stresses at the bottom of the tie were greater than design predictions but below 50% of the compressive strength of concrete.

The observed variability was not surprising. Although the upward jacking operation was conducted consistently, each arch had a different set of unknown forces in the hand-tightened hangers before the operation. Moreover, because the arches are highly indeterminate, different locked-in forces were expected in the hangers prior to upward jacking, depending on temperature and time-dependent effects. As a result, upward jacking, which was designed to change the forces in the hangers from an unknown initial state to a known final state, is expected to have variable effects on different arches. However, upward jacking tends to be more consistent than the sequential stressing of the hangers, which is the method commonly used for steel network arches. In sequential stressing, the same factors of variability will be present, in addition to more uncertainty regarding modeling assumptions and potential temperature changes that might happen during the time-consuming stressing of the hangers.

Stresses at the end of each construction operation

Figure 13 shows the stresses at the end of the main construction operations on the arches in the precasting yard. Design calculations were generally successful in predicting the stresses in the structure during precasting. While variability was observed in the concrete stresses between different arches, design calculations could identify the major parts of stress changes in the structure and provide safety for the arches during handling. The largest differences between measured and predicted stresses were observed at the bottom of the tie, where design predictions underestimated the compressive stresses. However, because the stresses were below the linearity limit of the concrete, such a difference should not be a source of concern.

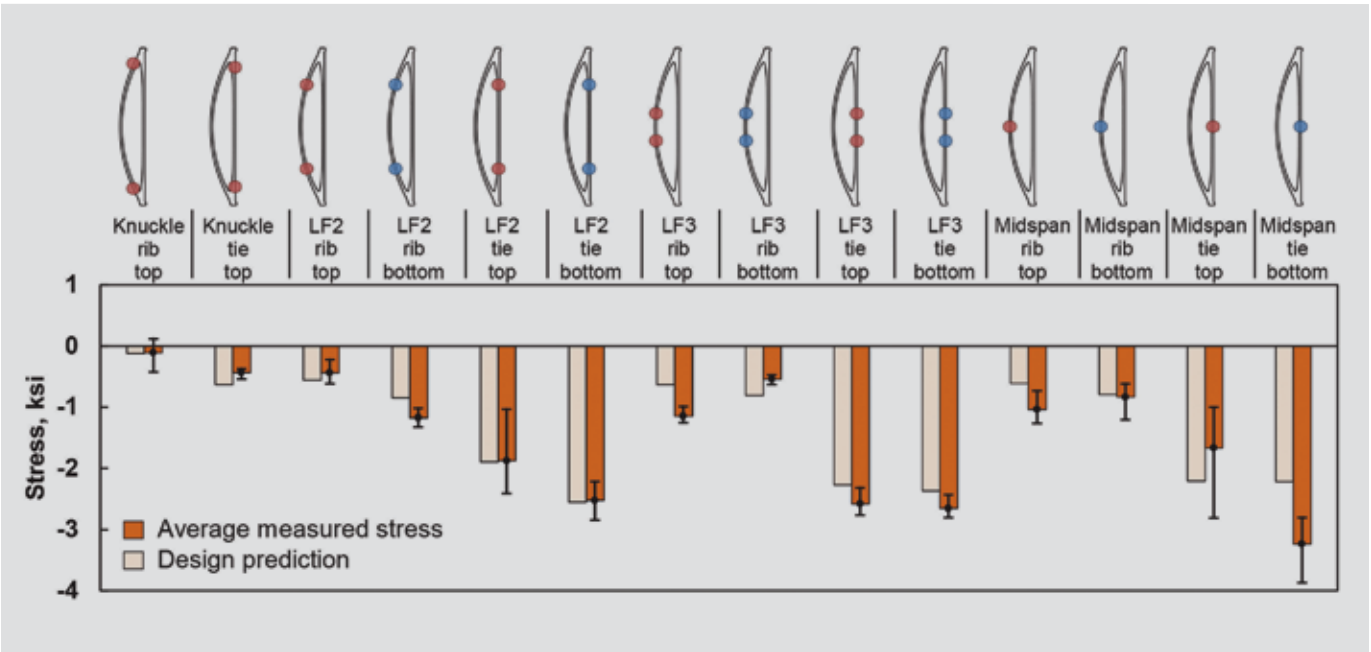

Figure 12. Maximum arch stresses during upward jacking operations, before deactivating the hydraulic rams. Note: The black lines show the range of observed stresses in different arches. 1 ksi = 6.895 MPa.

The total stresses in the finished bridge are highly influenced by the posttensioning and dead-load stresses. After the bridge was opened to traffic, a static live-load test was conducted on one of the most heavily instrumented spans of the bridge using four sand trucks, each weighing approximately 50 kip (220 kN). The largest live-load stress measured in the instrumented sections of the arches was approximately 0.20 ksi (1.4 MPa),[18] which is relatively small compared with the construction stresses in Fig. 13. The details of the live-load test on the bridge will be discussed in a later paper.

Conclusion

This paper evaluated the short-term stresses during construction of the first precast concrete network arch bridge in the world. The West Seventh Street Bridge was monitored using embedded vibrating-wire gauges throughout construction to develop an improved understanding of the structure's behavior and to ensure the safety of the arches. The primary conclusions of this paper are as follows:

- Design calculations were generally successful in capturing the essence of the structure's response during posttensioning and handling. As a result, the arches were successfully constructed without experiencing tensile stresses that could pose a risk of cracking or compressive stresses larger than 50% of the compressive strength of the concrete. The observed differences between average measured stresses and predicted stresses could be in part due to assumptions made regarding the modulus of elasticity of concrete in design calculations and the inherent complexities in converting the strain measurements to stresses.
- The short-term construction stresses in the identical arches could be highly variable from one arch to another, particularly after the arches were rotated into the vertical orientation. Uncertainties due to the presence of hand-tightened hangers and different temperature conditions among the arches may have contributed to such variability. In this project, the observed variability did not endanger the safety of the arches. However, reliable stress predictions for network arches must consider uncertainties due to unknown hanger conditions, regardless of the sophistication of the model. A successful handling design would best be obtained by assuming multiple conditions of hanger forces and making sure that the structure will not undergo excessive stresses due to an unforeseen stiffness distribution.
- Before finalizing the design of other structures that might be sensitive to cracking similar to these arches, a material study is highly recommended. The modulus of elasticity, creep, and shrinkage of the concrete will affect the stress. Therefore, these parameters must be realistically estimated before design. Although such a study is often impractical in initial design calculations, it is possible to analyze the model with the updated parameters once the final mixture is determined to verify the design.

To the authors' knowledge, the study presented herein is the first on the construction responses of a concrete tied arch bridge of any type. The data obtained in this study are a useful validation tool for future modeling of concrete arches.

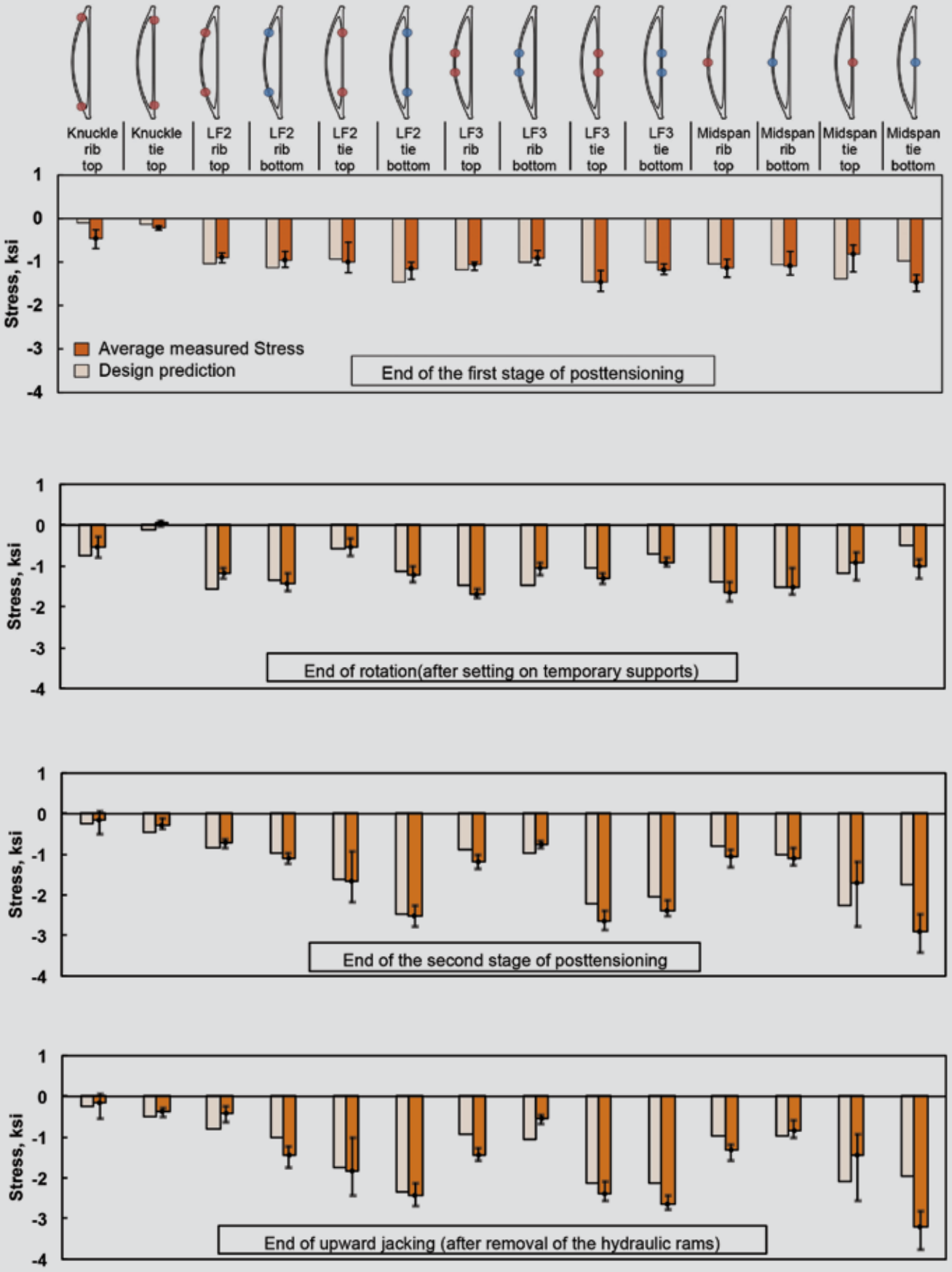

Figure 13. Stresses at the end of each construction operation. Note: The black lines show the range of observed stresses in different arches. 1 ksi = 6.895 MPa.

Acknowledgments

The authors gratefully acknowledge the Texas Department of Transportation (TxDOT) for providing financial support for this study. Dean Van Landuyt and Courtney Holle, the TxDOT engineers who designed the arches, provided a great deal of guidance. In addition, there were numerous engineers and representatives from TxDOT and the contractor, Sundt Construction, who provided significant assistance throughout the investigation. Many thanks are also due to Jose Gallardo, Ali Morovat, David Garber, Kostas Belivanis, Vasilis Samaras, and Hemal Patel, current and former graduate students at the University of Texas at Austin, for assisting with the instrumentation. The findings, opinions, and recommendations presented in this article are those of the authors and do not necessarily reflect the views of TxDOT.

References

1. Salonga, J. 2010. "Innovative Systems for Arch Bridges Using Ultra High-Performance Fibre-Reinforced Concrete." PhD thesis, University of Toronto, Toronto, ON, Canada.

2. Mondorf, P. 2006. "Arch Bridge Construction." In *Concrete Bridges*. 600–638. New York, NY: Taylor and Francis.

3. Tveit, P. 1987. "Considerations for Design of Network Arches." *ASCE Journal of Structural Engineering* 113 (10): 2189–2207.

4. Tveit, P. 2014. "Systematic Thesis on Network Arches." Accessed January 13, 2015. http://home.uia.no/pert/index.php/Systematic_Thesis.

5. Tveit, P. 2007. "An Introduction to the Optimal Network Arch." *Structural Engineering International* 17 (2): 184–187.

6. Tveit, P. 2010. "Optimal Network Arches for Road and Rail Bridges." In Proceedings of the 6th International Conference on Arch Bridges, College of Civil Engineering, Fuzhou University, Fuzhou, China. http://www.arch-bridges.com/paper2010/pdf/35-Optimal%20network%20arches%20for%20Road%20and%20rail%20bridges.pdf

7. Graβe, W., S. Teich, P. Tveit, and S. Wendelin. 2004. "Network Arches for Road Bridges." In Proceedings of the 4th International Conference on Arch Bridges, Barcelona, Spain. http://caminstech.upc.edu/sites/default/files/Network%20Arches%20for%20Road%20Bridges_0.pdf

8. Tveit, P. 2014. "The Network Arch: Bits of Manuscript in March 2014 after Lectures in 50+ Countries." Accessed January 13, 2015. http://home.uia.no/pert/index.php/The_Network_Arch.

9. Institute Stroyproekt JSC. 2014. "Ob River Crossing—Bugrinsky Bridge in Novosibirsk." Accessed January 13, 2015. http://www.stpr.ru/eng/projects/1045/.

10. Janata, V., D. Gregor, L. Šašek, P. Nehasil, and T. Wangler. 2012. "New Troja Bridge in Prague–Structural Solution of Steel Parts." *Procedia Engineering* 40: 159–164.

11. T. Zoli. 2012. "A Bridge by the People, for the People." *Civil Engineering: The Magazine of the American Society of Civil Engineers* 82 (6): 48–57.

12. Larssen, R. M., and S. E. Jakobsen. 2011. "Taller, Longer, Lighter: Meeting Growing Demand with Limited Resources." In *Proceedings of 35th Annual Symposium of IABSE/52nd Annual Symposium of IASS/6th International Conference on Space Structures. London, September 2011*. Switzerland: IABSE/IASS

13. Gauthier, P., and L. Krontal. 2010. "Erfahrungen mit Netzwerkbogenbrücken im Eisenbahnbrückenbau" [Experience with Network Arch Bridges in Railway Bridge Construction]. *Stahlbau* 79 (3): 199–208.

14. Wollmann, G., and T. Zoli. 2008. "Bridge across Ohio River and Blennerhassett Island." *Structural Engineering International* 18 (1): 28–30.

15. Mato, F. M., M. O. Cornejo, and J. N. Sánchez. 2011. "Design and Construction of Composite Tubular Arches with Network Suspension System: Recent Undertakings and Trends." *Journal of Civil Engineering and Architecture* 5 (3): 191–214.

16. Smit, T. 2013. "Design and Construction of a Railway Arch Bridge with a Network Hanger Arrangement." Master's thesis, Delft University of Technology, Delft, Netherlands.

17. Van Landuyt, D., C. Holle, and J. Aparicio. "Precast Network Arch Bridge." In *2013 PCI Convention and National Bridge Conference*. Chicago, IL: PCI. CD-ROM.

18. Yousefpour, H., T. Helwig, and O. Bayrak. 2014. "Structural Monitoring of the World's First Precast Network Arch Bridge during Construction." Center for Transportation Research technical report 5-5253-03-1. Austin, TX: University of Texas at Austin.

19. CEB (Comité Euro-International du Béton). 1993. *CEB-FIP Model Code 1990*. Lausanne, Switzerland: Thomas Telford.

20. AASHTO (American Association of State Highway and Transportation Officials). 2012. *AASHTO LRFD Bridge Design Speciafications*. 6th ed. Washington, DC: AASHTO.

21. Blok, J. 2012. "Stress Monitoring and Sweep Control Studies for Innovative Prestressed Precast Arches." Master's thesis, The University of Texas at Austin, Austin, TX.

22. Birrcher, D., R. Tuchscherer, M. Huizinga, O. Bayrak, S. Wood, and J. Jirsa. 2008. 'Strength and Serviceability Design of Reinforced Concrete Deep Beams." Center for Transportation Research technical report 0-5253-1. Austin, TX: University of Texas at Austin.

23. ASTM International. 2010. *Standard Test Method for Static Modulus of Elasticity and Poisson's Ratio of Concrete in Compression.* ASTM C469. West Conshohocken, PA: ASTM International.

24. ASTM International. 2012. *Standard Test Method for Compressive Strength of Cylindrical Concrete Specimens*. ASTM C39. West Conshohocken, PA: ASTM International.

25. ACI (American Concrete Institute) Committee 363. 2010. *Report on High-Strength Concrete*. ACI 363R-10. Farmington Hills, MI: ACI.

26. ASTM International. 2011. *Standard Practice for Estimating Concrete Strength by the Maturity Method*. ASTM C1074. West Conshohocken, PA: ASTM International.

27. Gardner, N. J., and M. Lockman. 2001. "Design Provisions for Drying Shrinkage and Creep of Normal-Strength Concrete." *ACI Materials Journal* 98 (2): 159–167.

Notation

E_c = modulus of elasticity of concrete

E_{ci} = modulus of elasticity of concrete at the time of the i^{th} construction operation

$f_c^{'}$ = compressive strength of concrete

R = radius of curvature

t = concrete age after casting

$\Delta\varepsilon_i$ = strain change in concrete due to the i^{th} construction operation

σ = stress in concrete

About the authors

Hossein Yousefpour is a PhD candidate in structural engineering at the University of Texas at Austin.

Todd A. Helwig, PhD, PE, is an associate professor in the Department of Civil, Architectural, and Environmental Engineering at the University of Texas at Austin. He holds the J. Neils Thompson Centennial Teaching Fellowship in Civil Engineering.

Oguzhan Bayrak, PhD, PE, is a professor in the Department of Civil, Architectural, and Environmental Engineering at the University of Texas at Austin. He holds the Charles Elmer Rowe Fellowship in the Cockrell School of Engineering and serves as the director of the Phil M. Ferguson Structural Engineering Laboratory.

Abstract

This paper reports some of the major findings from the instrumentation of the West Seventh Street Bridge in Fort Worth, Tex. This innovative bridge, completed in 2013 as a replacement for a century-old bridge, consists of 12 prestressed, precast concrete network arches. The bridge was instrumented with 224 vibrating-wire gauges that were embedded in the arches prior to concrete placement. The gauges were monitored during posttensioning, handling, and transport as well as deck construction. The instrumentation provided data on the stresses induced in the arches, which were used to ensure a safe environment throughout construction. The measurements also provided a means for evaluating the accuracy of stress calculations that were made during design. The results obtained from this study provide a unique insight into the behavior of concrete arches built by an accelerated construction method.

Keywords

Accelerated bridge construction, arch, bridge, monitoring, network arch, post tensioning.

Review policy

This paper was reviewed in accordance with the Precast/Prestressed Concrete Institute's peer-review process.

Reader comments

Please address reader comments to journal@pci.org or Precast/Prestressed Concrete Institute, c/o *PCI Journal*, 200 W. Adams St., Suite 2100, Chicago, IL 60606.